RSC Medicinal Chemistry

ROYAL SOCIETY OF CHEMISTRY

RESEARCH ARTICLE

Published on 26 August 2024
Licence and permissions

Check for updates

Cite this: *RSC Med. Chem.*, 2024, **15**, 3704

Preventing SARS-CoV-2 infection using Fv-antibodies targeting the proprotein convertase (PPC) cleavage site

Jaeyong Jung,[a] Jeong Soo Sung,[a] Soonil Kwon,[a] Hyung Eun Bae,[a] Min-Jung Kang,[c] Joachim Jose,[d] Misu Lee*[be] and Jae-Chul Pyun*[a]

Received 17th July 2024,
Accepted 23rd August 2024

DOI: 10.1039/d4md00552j

rsc.li/medchem

Fv-antibodies targeting the proprotein convertase (PPC) region of the SARS-CoV-2 spike protein (SP) were screened from an Fv-antibody library to inhibit SARS-CoV-2 infection. Two selected Fv-antibodies were expressed as soluble recombinant proteins, and their binding affinities were assessed using a surface plasmon resonance biosensor. The binding regions of these Fv-antibodies corresponded to the cleavage sites of furin (S1/S2) and transmembrane serine protease 2 (TMPRSS2, S2′). The neutralizing activities of the two Fv-antibodies were demonstrated using a cell-based infection assay with pseudo-viruses carrying the SP of four different SARS-CoV-2 variants: wild-type (D614), delta (B.1.617.2), omicron (BA.2), and omicron (BA.4/5).

1. Introduction

The infection process of severe acute respiratory syndrome coronavirus 2 (SARS-CoV-2) begins with the binding of the spike protein (SP) to the angiotensin-converting enzyme 2 (ACE2) receptor.[1–3] For SARS-CoV-2 to further infect the host cell membrane, the spike protein must be cleaved at two regions known as S1/S2 (residues: 682–685) and S2′ (residues: 809–815), referred to as proprotein convertase (PPC) sites.[4,5] The proteolytic enzymes furin (S1/S2) and transmembrane serine protease 2 (TMPRSS2, S2′) are responsible for cleaving these sites, respectively.[6,7] Due to the highly conserved amino acid sequences in these regions among coronaviruses, antibodies targeting these sites have been developed to prevent SARS-CoV-2 infection.[8–11] However, accessing these regions with antibodies is challenging due to steric hindrance from the spike protein structure around the PPC region.[12] To overcome the steric hindrance in accessing the PPC region, many research groups have developed small molecules with binding affinity to these sites as pan-corona drugs.[13–15] In this study, Fv-antibodies with high binding affinity to the PPC region were screened from an Fv-antibody library to prevent SARS-CoV-2 infection, as illustrated in Scheme 1. Fv-antibodies are derived from the V_H region of immunoglobulin G (IgG), which consists of three complementarity-determining regions (CDR1-3) and four framework regions (FR1-4).[16,17] The Fv-antibody library was produced by randomizing CDR3 (11 amino acid residues) through site-directed mutagenesis. The prepared Fv-antibody library was expressed on the outer membrane of *E. coli* using autodisplay technology.[3,10,18–21]

This method utilizes the AIDA-1 to transport the expressed target proteins through its beta-barrel.[22] The prepared Fv-antibody library exhibited a high surface density of 10^5 Fv-antibodies per *E. coli* and a diversity of 10^6 Fv-antibodies per library. The Fv-antibodies were screened using the amino acid sequence of the PPC region (residue: 661–900), which includes two cleavage sites, as the screening probe. The selected Fv-antibodies were expressed as soluble proteins, and their binding activities to the PPC region (S1/S2 and S2′, respectively) were evaluated. Finally, the neutralizing activity

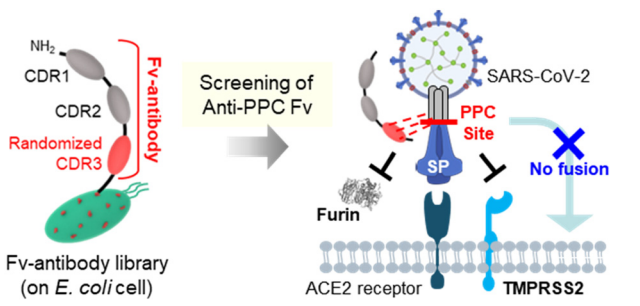

Scheme 1 Fv-antibodies targeting the PPC region of SARS-CoV-2 to prevent infection, screened from an Fv-antibody library.

[a] *Department of Materials Science and Engineering, Yonsei University, 50 Yonsei-ro, Seodaemun-gu, Seoul, 03722, Korea. E-mail: jcpyun@yonsei.ac.kr*
[b] *Division of Life Sciences, College of Life Science and Bioengineering, Incheon National University, Incheon, 22012, Korea. E-mail: misulee@inu.ac.kr*
[c] *Korea Institute of Science and Technology (KIST), Seoul, 02456, Korea*
[d] *Institute of Pharmaceutical and Medical Chemistry, Westfälischen Wilhelms-Universität Münster, Muenster, Germany*
[e] *Institute for New Drug Development, College of Life Science and Bioengineering, Incheon National University, Incheon, 22012, Korea*

of these Fv-antibodies was tested using pseudo-virus particles with the SP of four different SARS-CoV-2 variants: wild-type (D614), delta (B.1.617.2), omicron (BA.2), and omicron (BA.4/5).[23,24] This evaluation included measuring their ability to prevent the virus from binding to host cells that express the ACE2 receptor and TMPRSS2.

2. Results and discussion

2.1 Screening of Fv-antibodies against PPC region

The Fv-antibody library was generated by introducing random mutation into the 11 amino acid residues of CDR3 region using site-directed mutagenesis, as shown in Fig. 1(a). The Fv-antibody library was screened and expressed as a probe, incorporating the PPC region of the SP, which is known to have a highly conserved amino acid sequence among coronaviruses. The PPC region, including S1/S2 and S2′ (amino acid sequence 661–900, 240 residues) within the SP (residues: 1–1273), were expressed as a fusion protein with GFP (53.6 kDa), as shown in Fig. 1(b).[9,23] Screening for Fv-antibodies against the PPC region involved isolating *E. coli* clones bound to the PPC probe using flow cytometry. As illustrated in Fig. 1(c), the dot plots of the Fv-antibody library revealed a highly fluorescent region compared to the control strain (expressing only autodisplayed CDR1 and CDR2) and intact *E. coli*, indicating *E. coli* clones with binding affinity to the PPC region.[19] The highly fluorescent *E. coli* clones were isolated and cultured on LB agar plates. Clones with high binding affinity for the PPC probe were selected, and the final clones were determined after sequencing the oligonucleotide of the CDR3 region. Two clones with target Fv-antibodies against the PPC region were identified as the final clones (Fig. 1(d)). Detailed information on these Fv-antibodies, including oligonucleotide sequences, corresponding amino acid sequences, and binding affinities, is summarized in Table 1.

2.2 Characteristic of screened anti-PPC Fv-antibodies

The screened Fv-antibodies were expressed as soluble GFP proteins (Fig. 2(a)). The binding affinities (K_D) were estimated to be 38.0 nM for anti-PPC Fv1 (from screened clone-1) and 42.9 nM for anti-PPC Fv2 (from screened clone-2) using an SPR biosensor with an immobilized PPC probe on an Au chip (Fig. 2(b)).[25] Considering that the binding affinity of the enzyme furin for the S1/S2 cleavage region is known to be 16 nM,[26] the binding affinities of the Fv-antibodies were deemed sufficient to effectively target the PPC region. To analyze the binding regions of each Fv-antibody, docking simulations were performed using Autodock Vina from Scripps Research (La Jolla, CA, USA)[27] and the structure of the PPC region of SP (PDB 6ZP5). As shown in Fig. 2(c), the amino acids of the PPC site binding with anti-PPC Fv1 hydrogen interactions were designated to be S^{7} (CDR3)–R^{683} (PPC).

For hydrophobic bonding, the following amino acids were analyzed to be involved: R^{3}–P^{665}, A^{4}–I^{664} and I^{666}. The amino acids of the PPC site binding with anti-PPC Fv2 involved in

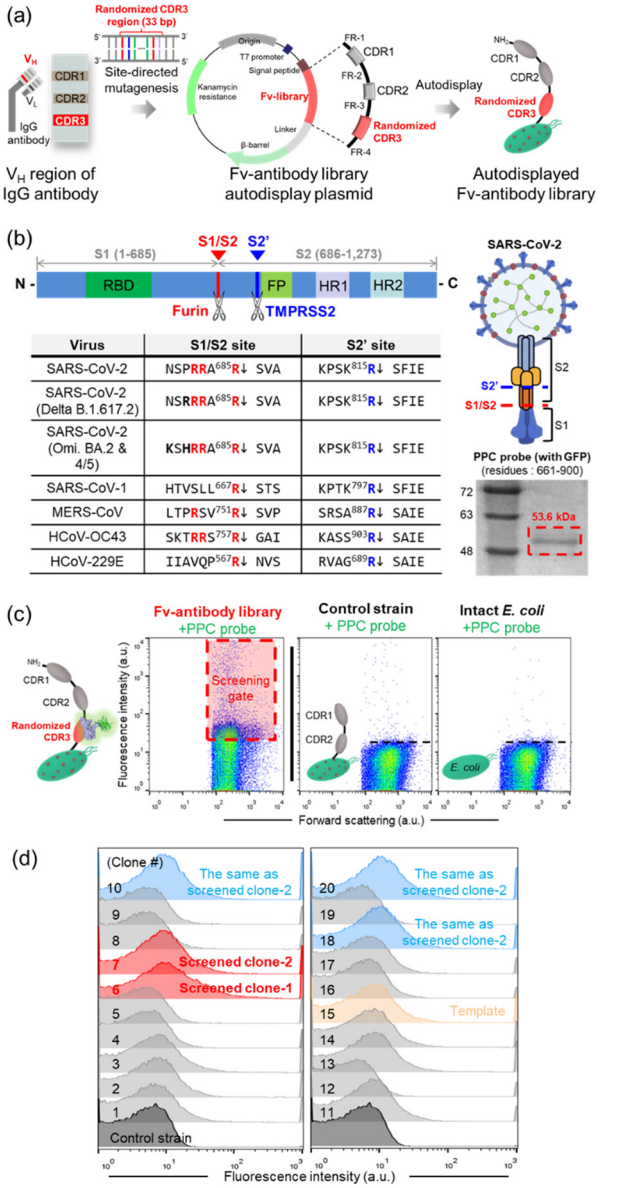

Fig. 1 Screening Fv-antibodies with specific binding affinity to the SARS-CoV-2 PPC region from an Fv-antibody library. (a) Preparation of the Fv-antibody library on the surface of *E. coli*. (b) Analysis of the SARS-CoV-2 PPC sites (S1/S2: 682–685, S2′: 809–815), which have highly conserved amino acid sequences among coronaviruses, and expression of the SARS-CoV-2 PPC probe (residues 661–900) as a GFP fusion protein. (c) Screening of clones with binding affinity to the SARS-CoV-2 PPC probe. (d) Analysis of SARS-CoV-2 PPC probe activity in the screened clones.

hydrophobic interactions were assigned as R^{6}–P^{809}, R^{7}–P^{807} and P^{809}, R^{8}–P^{793}, F^{11}–K^{790} and P^{809}. From the measurement with SPR biosensor, binding affinities (K_D) of screened Fv-antibodies were estimated to be 3.8×10^{-8} M for anti-PPC Fv1 and 4.2×10^{-8} M for anti-PPC Fv2. From the docking simulation, the ΔG values were calculated −8.0 for anti-PPC Fv1 and −8.7 M for anti-PPC Fv2, respectively. The dissociation constant K_D is related to the Gibbs free energy change (ΔG) by the following equation:

Table 1 Oligonucleotide and amino acid sequences of Fv-antibodies and their binding affinities (K_D) to the SARS-CoV-2 PPC region

Screened clone	CDR3 region sequence		Binding constant (K_D)
	Oligonucleotide (33 bp)	Amino acid (11 mer)	SPR (nM)
1	5′-GAC GGT CGT GCT CGC CAA AGC CAG GAT GAT GAT-3′	^{1}DGRAR ^{5}QSQDD ^{11}D	38.0
2	5′-GGC AGC CAA ATC GCT CTT CGG CGG AGG GAT TTC-3′	^{1}GSQIA ^{5}LRRRD ^{11}F	42.9

$$K_D = \exp\left(\frac{\Delta G}{RT}\right),$$

where ΔG represented the Gibbs free energy change (kcal mol^{-1}) and R represented the gas constant (0.001987 kcal mol^{-1} × K) and T represented the absolute temperature (Kelvin).[28] Considering the above equation, the K_D value of anti-PPC Fv1 and Fv2 is as followers: $K_D = 8.7 \times 10^{-7}$ M for anti-PPC Fv1 and 2.6×10^{-7} M for anti-PPC Fv2. In comparison with binding affinities (K_D) from the SPR measurement, the calculated K_D values from the docking simulation were considered to be comparable level. Each Fv-antibody was analyzed to determine the cleavage sites for different proteolytic enzymes. Anti-PPC Fv1 was found to bind near the furin cleavage site (residues: 682–685), while anti-PPC Fv2 bound near the TMPRSS2 cleavage site (residues: 809–815).[6,29] The binding of Fv-antibodies at the analyzed sites was further investigated by performing cleavage reactions with the PPC probe and furin after treatment with each Fv-antibody. These cleavage reactions were conducted by varying the concentration of the Fv-antibodies while keeping the concentration of the PPC probe and furin constant. As shown in Fig. 2(d), the PPC probe (protein band at 53.6 kDa) was not cleaved by furin, indicating that the S1/S2 region was blocked by the binding of anti-PPC Fv1. The inhibition activity (IC_{50}) was calculated to be 709.5 nM for anti-PPC Fv1.[30] In contrast, when treated with anti-PPC Fv2, the PPC probe was cleaved, demonstrating that furin cleavage remained active despite anti-PPC Fv2 treatment. As previously mentioned, anti-PPC Fv2 binds to the TMPRSS2 cleavage site, and therefore, it could not block furin cleavage of the PPC probe. The binding of anti-PPC Fv2 to the S2′ site was confirmed using an SPR biosensor. The PPC probe, containing both S1/S2 and S2′ sites, was immobilized on an Au chip, and anti-PPC Fv2 treatment produced a significant SPR signal, indicating binding. However, sequential treatment with the TMPRSS2 binding domain and anti-PPC Fv2 produced an insignificant SPR signal, as shown in Fig. 2(e). These results confirm that anti-PPC Fv2 has an affinity for the S2′ site of the PPC probe. The study demonstrated that Fv-antibodies bind to different cleavage sites in the PPC region of various proteolytic enzymes.

2.3 Neutralization activity of anti-PPC Fv-antibodies against SARS-CoV-2 infection

The neutralizing activity of these Fv-antibodies was assessed using a cell-based infection assay with pseudo-virus particles.[23,24,31]

HEK293T cells stably expressing human ACE2 receptor and TMPRSS2 were used as host cells. Pseudo-virus particles were prepared using lentivirus expressing the SP of SARS-CoV-2 variants: wild-type (D614), delta (B.1.617.2), omicron (BA.2), and omicron (BA.4/5). These particles contained a GFP expression vector, which fluoresced upon infection of the host cells. As shown in Fig. 3(a), fluorescence was detected in host cells infected by pseudo-virus particles. However, when anti-PPC Fv prevented viral infection, no fluorescence signal was observed. Thus, the neutralizing activity of the Fv-antibodies was measured based on the fluorescence of the host cells. The *in vitro* cell-based infection assay was carried out at the concentration of Fv-antibodies corresponding to their binding affinity (K_D) to compare the neutralizing activity of these Fv-antibodies at the same binding condition. The binding affinities (K_D) of these Fv antibodies were measured to be 3.8×10^{-8} M for anti-PPC Fv1 and 4.2×10^{-8} M for anti-PPC Fv2 using SPR measurement (Fig. 2(b)). As shown in Fig. 3(b), the cell-based infection assay showed decreased fluorescence signals from host cells after treatment of Fv-antibodies. These results showed that two kinds of Fv-antibodies had the neutralizing activity against the infection of four kinds of pseudo-virus expressing the SP of SARS-CoV-2 variants. As shown in Fig. 3(c), the neutralizing activity was quantified by measuring the fluorescence signal using flow cytometry. The neutralizing activity against pseudo-virus particles (wild-type) was estimated to be −89.7% for anti-PPC Fv1 and −85.7% for Fv2. The high neutralizing activity of anti-PPC Fv1 and Fv2 was attributed to their binding to the cleavage sites of furin and TMPRSS2, respectively (Fig. 2(c)). The neutralizing activity of the two Fv-antibodies was similarly high (−72.6–−89.7%) for other pseudo-virus particles. These results demonstrate that Fv-antibodies effectively inhibit the activity of furin and TMPRSS2 by binding to their respective cleavage sites. These results indicate that neutralizing antibodies targeting the PPC region could be effectively utilized to prevent SARS-CoV-2 infection, as the coronavirus family exhibits a highly conserved amino acid sequence at this site.

3. Conclusions

In this study, Fv-antibodies specific to the PPC region were screened from the Fv-antibody library generated through site-directed mutagenesis of the CDR3 region. The Fv-antibody library was displayed on the outer membrane of *E. coli* using autodisplay technology, achieving an expression level of $>10^5$ Fv-antibodies per *E. coli* with a diversity of $>10^6$ Fv-

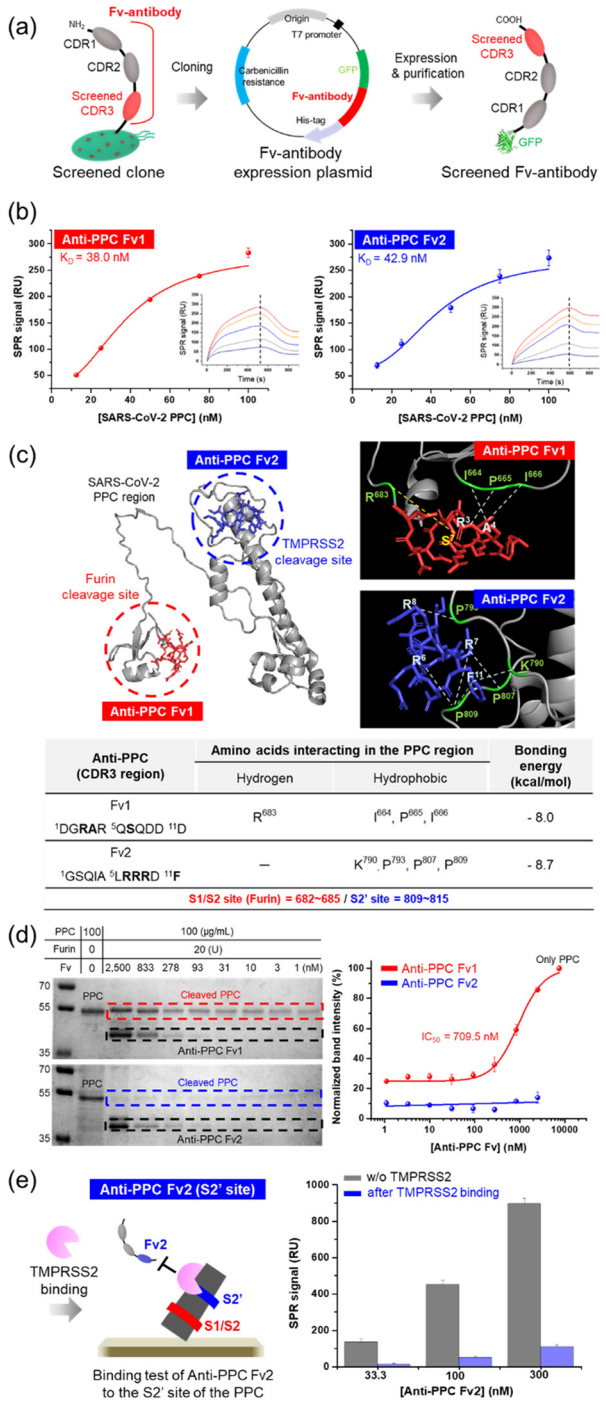

Anti-PPC (CDR3 region)	Amino acids interacting in the PPC region		Bonding energy (kcal/mol)
	Hydrogen	Hydrophobic	
Fv1 ^{1}DG**RAR** ^{5}**QS**QDD ^{11}D	R^{683}	I^{664}, P^{665}, I^{666}	- 8.0
Fv2 ^{1}GSQIA ^{5}**LRRR**D ^{11}F	—	K^{790}, P^{793}, P^{807}, P^{809}	- 8.7

S1/S2 site (Furin) = 682~685 / S2' site = 809~815

Fig. 2 Analysis of the binding affinity of expressed Fv-antibodies (anti-PPC Fv1 and Fv2). (a) Schematic for the expression of screened Fv-antibodies. (b) Estimation of the binding affinity (K_D) of the anti-PPC Fv using an SPR biosensor. (c) Docking simulation analysis of the binding sites of anti-PPC Fv to the PPC region. (d) Furin-mediated PPC cleavage inhibition assay using anti-PPC Fv. (e) SPR biosensor analysis of anti-PPC Fv2 binding to the S2′ site.

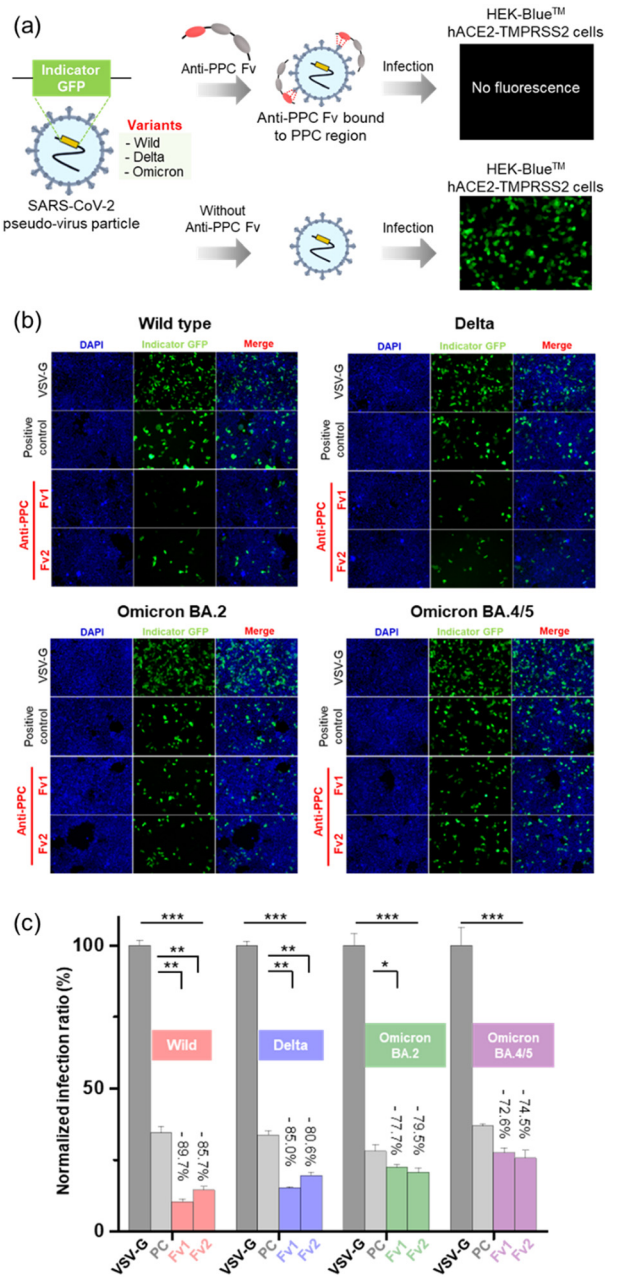

Fig. 3 *In vitro* cell-based infection assay. (a) *In vitro* cell-based infection assay using pseudo-virus particles with spike proteins from four different SARS-CoV-2 variants: wild type (D614), delta (B.1.617.2), omicron (BA.2), and omicron (BA.4/5). (b) Inhibition analysis using anti-PPC Fv and pseudo-virus particles, demonstrated through fluorescence imaging. (c) Estimation of the inhibition ratio of SARS-CoV-2 infection.

antibodies per library. Following screening, the Fv-antibodies were produced as soluble recombinant proteins. The SPR biosensor was used to determine the K_D of the screened Fv-antibodies, with anti-PPC Fv1 and Fv2 estimated to have affinities 38.0 nM and 42.9 nM, respectively. These Fv-antibodies specifically bind to the S1/S2 and S2′ cleavage sites of furin and TMPRSS2, respectively, effectively blocking these regions. The neutralizing activity of the anti-PPC Fv-antibodies against the PPC region was evaluated using an *in vitro* cell-based infection assay with pseudo-virus expressing the SP of SARS-CoV-2 variants: wild-type (D614), delta (B.1.617.2), omicron (BA.2), and omicron (BA.4/5) and host cells expressing ACE2 receptor and TMPRSS2. The

neutralizing activity of anti-PPC Fv-antibodies ranged from −72.6% to −89.7% compared to VSV-G virus infection. These results indicate that the screened anti-PPC Fv effectively inhibit the activity of furin and TMPRSS2 by binding to their respective cleavage sites, even in the presence of mutations in the SP.

4. Experimental section

4.1 Materials

The SARS-CoV-2 proprotein convertase (PPC) region (residues 661–900, 53.6 kDa) and the transmembrane serine protease 2 (TMPRSS2) region (residues 106–492, 69.7 kDa) were custom-synthesized as a fusion protein with labeled green fluorescent protein (GFP) at N-terminal by Cosmo Genetech (Seoul, South Korea).[32,33] Luria–Bertani medium was obtained from Duchefa (Haarlem, Netherlands). DNA oligonucleotides for Fv-antibody library production were synthesized by Bionics (Seoul, South Korea). Furin was obtained from Sigma-Aldrich (St. Louis, MO, USA). Materials related to SARS-CoV-2 variant pseudo-virus production were described in a previous study.[23] Pseudotyping SP variant vectors and HEK-Blue™ cells (overexpressing hACE2-TMPRSS2) were obtained from InvivoGen Inc. (San Diego, CA, USA). Dulbecco's modified Eagle medium (DMEM) and Opti-MEM were obtained from Gibco Inc. (Waltham, MA, USA).

4.2 Screening of anti-PPC Fv from Fv-antibody library

The preparation of the Fv-antibody library has been described in previous studies.[3,18,19,23] Clones exhibiting binding activity to the PPC region probe were screened from the Fv-antibody library as follows: (1) the randomized CDR3 region of the Fv-antibody was expressed on the membrane of *E. coli*. (2) PPC region probe (1 μM, 100 μL) was treated with the Fv-antibody library (100 μL) for 1 h at 37 °C. (3) After washing with PBS containing 0.01% Tween 20, screened clones with binding activity to PPC probe were sorted (n = 500) using a screening gate on a flow cytometer (FACSCalibur™, NJ, USA). (4) Screened clones were selected after testing activity with PPC probe and identifying the CDR3 region using DNA oligonucleotide sequencing.

4.3 Purification and preparation of anti-PPC Fv

The screened Fv-antibody expression plasmid was designed to express a fusion protein with fluorescent tags (GFP or tdTomato) at the N-terminal. This plasmid was synthesized by Cosmo Genetech (Seoul, Korea). The sequences of the CDR3 region were listed in detail in Table 1. The purification of Fv-antibody was carried out as follows: competent BL21(DE3) *E. coli* cells were transformed with the Fv-antibody expression plasmid. The transformed *E. coli* cells were then cultured in 10 mL Luria–Bertani (LB) medium containing 1 mM isopropyl β-D-1-thiogalactopyranoside (IPTG) for 16 h at 30 °C. The cultured *E. coli* cells were harvested by centrifugation at 5000g for 3 min and resuspended in 20 mL of binding buffer (3 M urea, 5 mM Tris–HCl and 0.5 M NaCl). The resuspended cells were lysed by sonication (Vibra cell VCX-130) for 10 min with 5 s on/off cycles, and the lysate was subsequently centrifuged at 22 500g for 10 min. The Fv-antibodies present in the supernatant were purified using a His-tag column. Finally, the purified Fv-antibodies were gradually dialyzed to remove urea and imidazole using membrane filter for 16 h at 4 °C.

4.4 K_D estimation of anti-PPC Fv

The K_D of the anti-PPC Fv was determined using an SPR biosensor (i-ClueBio, Seongnam, South Korea). The SPR chips, composed of BK-7 glass, were coated with a 2 nm titanium layer followed by a 48 nm gold layer. Anti-PPC Fv was immobilized on the gold surface. Anti-PPC Fv (20 μg mL^{-1}, 100 μL) was incubated on the SPR chips for 16 h at 4 °C. Subsequently, the SPR chips were blocked using BSA (1 mg mL^{-1}) for 1 h at 37 °C. After washing with PBS containing 0.01% Tween 20, PPC antigen concentrations ranging from 12.5 to 100.0 nM were introduced at a flow rate of 25 μL min^{-1} for 10 min to promote binding. To facilitate dissociation, the washing buffer (PBS) was allowed to flow for 10 min at the same rate.

4.5 Analysis of furin-mediated PPC cleavage inhibition

To analyze whether anti-PPC Fv1 binds to the PPC region and inhibits furin cleavage (S1/S2 site), the Fv-antibodies were incubated with a fixed concentration of PPC and furin. After mixing PPC (100 μg mL^{-1}) with furin (20 units), the anti-PPC Fv1 (targeting the S1/S2 site) and Fv2 (targeting the S2′ site) were added at concentrations ranging from 1 to 2500 nM and incubated at 37 °C for 1 h, respectively. The reacted samples were analyzed using SDS-PAGE, and the band intensity was quantified using ImageJ software.

4.6 Analysis of anti-PPC Fv2 binding to the S2′ site

The binding of anti-PPC Fv2 to the S2′ site was confirmed using the SPR biosensor. SPR measurements were performed as described above. Immobilization of the PPC probe (20 μg mL^{-1}, 100 μL) onto the gold surface was carried out. TMPRSS2 (100 nM) was introduced to bind to the S2′ site of the PPC probe. After washing with PBS, anti-PPC Fv1 (targeting the S1/S2 site) and Fv2 (targeting the S2′ site) were reacted at concentrations ranging from 33.3 to 300.0 nM, respectively.

4.7 Production of pseudo-viral particles

Production of SARS-CoV-2 SP variant pseudo-virus (wild-type D614, delta B.1.617.2, omicron BA.2, and omicron BA.4/5) was carried out using Lenti-X™ HEK293T cells. Pseudoviral particles were generated as follows: (1) Lenti-X™ HEK cells (1×10^5 cells) were cultured in 15 mL of DMEM containing 10% FBS for 1 d. (2) Transfection reagent (FuGENE, 10 μL) was mixed with 5 μg of each plasmid (SARS-CoV-2 SP pseudotyping vectors, pLVXS-ZsGreen1-Puro, and psPAX2) in

1 mL of Opti-MEM and incubated at 37 °C for 10 min. (3) The medium was replaced with 10 mL DMEM containing 10% FBS, and the mixture (1 mL Opti-MEM) from step 2 was added to the cells. (4) After 3 d of incubation, the supernatant was collected by centrifugation (500×*g*, 10 min). (6) Lenti-X™ concentrator was added to the supernatant and incubated for 3 h at 4 °C. (7) Particles were collected by centrifugation (1500×*g*, 45 min) and supplemented with DMEM. (8) The titers of the pseudo-viral particles were estimated using Lenti-X™ qRT-PCR, yielding results between 10^8 and 10^9 copies per mL.

4.8 Neutralization assay using anti-PPC Fv

The neutralizing activity of screened Fv-antibodies were evaluated using an *in vitro* cell-based infection assay. HEK-Blue™ cells (overexpressing hACE2 and TMPRSS2, 5.0×10^4/well) were plated onto 96-well microplates coated with poly-L-lysine and incubated in a CO_2 incubator for 1 d at 37 °C. The Fv-antibodies were incubated with the pseudo-viral particles for 30 min at 37 °C in 100 μL of DMEM containing 2% FBS. Subsequently, pseudoviral particles pre-incubated with anti-PPC Fv were added to HEK-Blue™ cells and incubated for 48 h. Cell images were captured using a fluorescence microscope (Nikon, Eclipse Ts2, Tokyo, Japan).

Data availability

The data used in this article can be available upon request to the corresponding author.

Conflicts of interest

There are no conflicts to declare.

Acknowledgements

This work was supported by the National Research Foundation of Korea (grant numbers: RS-2023-00209053, NRF-2020R1A5A101913111, NRF-2022R1A2C1007956 and NRF-2022K1A3A1A25081295) and the Korea Health Industry Development Institute (KHIDI) of Korea (RS-2022-KH128357(HV22C0131)).

References

1 J. Yang, S. J. Petitjean, M. Koehler, Q. Zhang, A. C. Dumitru, W. Chen, S. Derclaye, S. P. Vincent, P. Soumillion and D. Alsteens, *Nat. Commun.*, 2020, **11**, 4541.
2 J. Lan, J. Ge, J. Yu, S. Shan, H. Zhou, S. Fan, Q. Zhang, X. Shi, Q. Wang, L. Zhang and X. Wang, *Nature*, 2020, **581**, 215–220.
3 J. Jung, J.-H. Bong, J. S. Sung, J.-H. Park, T.-H. Kim, S. Kwon, M.-J. Kang, J. Jose and J.-C. Pyun, *Biosens. Bioelectron.*, 2023, **237**, 115439.
4 J. Shang, Y. Wan, C. Luo, G. Ye, Q. Geng, A. Auerbach and F. Li, *Proc. Natl. Acad. Sci. U. S. A.*, 2020, **117**, 11727–11734.
5 Y. K. Lee and H. S. Song, *BioChip J.*, 2024, **18**, 171–185.
6 D. Bestle, M. R. Heindl, H. Limburg, O. Pilgram, H. Moulton, D. A. Stein, K. Hardes, M. Eickmann, O. Dolnik and C. Rohde, *Life Sci. Alliance*, 2020, **3**, e202000786.
7 M. Hoffmann, H. Kleine-Weber, S. Schroeder, N. Krüger, T. Herrler, S. Erichsen, T. S. Schiergens, G. Herrler, N.-H. Wu and A. Nitsche, *Cell*, 2020, **181**, 271–280.e278.
8 S. Xiu, A. Dick, H. Ju, S. Mirzaie, F. Abdi, S. Cocklin, P. Zhan and X. Liu, *J. Med. Chem.*, 2020, **63**, 12256–12274.
9 S. Kim and J.-H. Lee, *BioChip J.*, 2022, **16**, 376–396.
10 J. Jung, J. S. Sung, T.-H. Kim, M.-J. Kang, J. Jose, H.-J. Shin and J.-C. Pyun, *BioChip J.*, 2024, **18**, 318–329.
11 K. H. Kim, Y. K. Yoo, N. E. Lee, J. Lee, C. Kim, S. Lee, J. Kim, S. J. Park, D. Lee and S. W. Lee, *BioChip J.*, 2023, **17**, 340–348.
12 K. Al Adem, A. Shanti, C. Stefanini and S. Lee, *Pharmaceuticals*, 2020, **13**, 447.
13 H. Su, F. Zhou, Z. Huang, X. Ma, K. Natarajan, M. Zhang, Y. Huang and H. Su, *Angew. Chem.*, 2021, **133**, 9873–9886.
14 S. Mediouni, H. Mou, Y. Otsuka, J. A. Jablonski, R. S. Adcock, L. Batra, D.-H. Chung, C. Rood, I. M. S. de Vera and R. Rahaim Jr, *SLAS Discovery*, 2022, **27**, 8–19.
15 V. Tiwari, J. C. Beer, N. V. Sankaranarayanan, M. Swanson-Mungerson and U. R. Desai, *Drug Discovery Today*, 2020, **25**, 1535–1544.
16 J. Lu, T. Panavas, K. Thys, J. Aerssens, M. Naso, J. Fisher, M. Rycyzyn and R. W. Sweet, *Mol. Immunol.*, 2014, **57**, 274–283.
17 S. D'Angelo, F. Ferrara, L. Naranjo, M. F. Erasmus, P. Hraber and A. R. Bradbury, *Front. Immunol.*, 2018, **9**, 395.
18 J. S. Sung, Y. Han, T. G. Yun, J. Jung, T.-H. Kim, F. Piccinini, M.-J. Kang, J. Jose, M. Lee and J.-C. Pyun, *Int. J. Biol. Macromol.*, 2024, **265**, 130854.
19 J. S. Sung, S. Kim, J. Jung, T.-H. Kim, S. Kwon, H. E. Bae, M.-J. Kang, J. Jose, M. Lee and J.-C. Pyun, *ACS Pharmacol. Transl. Sci.*, 2023, **7**, 150–160.
20 J. S. Sung, J.-H. Bong, T. G. Yun, Y. Han, Y. Park, J. Jung, S. J. Lee, M.-J. Kang, J. Jose and M. Lee, *Bioconjugate Chem.*, 2022, **33**, 1166–1178.
21 J. S. Sung, J. Jung, H. Hwang, J.-H. Bong, M.-J. Kang, J. Jose, M. Lee and J.-C. Pyun, *ACS Pharmacol. Transl. Sci.*, 2023, **6**, 1945–1957.
22 J. Jose and T. F. Meyer, *Microbiol. Mol. Biol. Rev.*, 2007, **71**, 600–619.
23 J. Jung, J. S. Sung, J.-H. Bong, T.-H. Kim, S. Kwon, H. E. Bae, M.-J. Kang, J. Jose, M. Lee and H.-J. Shin, *Biosens. Bioelectron.*, 2023, **245**, 115834.
24 M. Lee, B. Kang, J. Lee, J. Lee, S. T. Jung, C. Y. Son and S. S. Oh, *Sci. Adv.*, 2022, **8**, eabq6207.
25 J.-H. Bong, S. J. Lee, J. Jung, J. S. Sung, M.-J. Kang, M. Lee, J. Jose and J.-C. Pyun, *BioChip J.*, 2024, **18**, 146–159.
26 A. Mohammad, E. Alshawaf, S. K. Marafie, M. Abu-Farha, J. Abubaker and F. Al-Mulla, *Int. J. Infect. Dis.*, 2021, **103**, 611–616.
27 J. Eberhardt, D. Santos-Martins, A. F. Tillack and S. Forli, *J. Chem. Inf. Model.*, 2021, **61**, 3891–3898.
28 S. Kumar, D. Bose, H. Suryawanshi, H. Sabharwal, K. Mapa and S. Maiti, *PLoS One*, 2011, **6**, e23300.

29 Q. Zhang, R. Xiang, S. Huo, Y. Zhou, S. Jiang, Q. Wang and F. Yu, *Signal Transduction Targeted Ther.*, 2021, **6**, 233.
30 P. Larsson, H. Engqvist, J. Biermann, E. W. Rönnerman, E. Forssell-Aronsson, A. Kovács, P. Karlsson, K. Helou and T. Z. Parris, *Sci. Rep.*, 2020, **10**, 5798.
31 J. Nie, Q. Li, J. Wu, C. Zhao, H. Hao, H. Liu, L. Zhang, L. Nie, H. Qin and M. Wang, *Emerging Microbes Infect.*, 2020, **9**, 680–686.
32 M. Zimmer, *Chem. Rev.*, 2002, **102**, 759–782.
33 J.-D. Pédelacq, S. Cabantous, T. Tran, T. C. Terwilliger and G. S. Waldo, *Nat. Biotechnol.*, 2006, **24**, 79–88.

